Accurate Modeling Methods and Optimization of Parasitic Capacitances in MHz-Level WPT Magnetically Coupled Planar Spiral Coils

Qing HE, Wei CHEN, Chezu WANG, Wei QIU, and Qingbin CHEN

***Abstract*—Once the operating frequency of magnetic coupling resonant wireless power transfer (MCR-WPT) reaches the MHz level, the capacitive parasitic parameters of the coils will affect the transmission capacity of the series/series (S/S) compensated WPT. In this paper, by establishing a mathematical model of the parasitic equivalent capacitance in the coil, it is pointed out that the parasitic equivalent capacitance is determined by both the coil structure (including the structural capacitance between adjacent and non-adjacent turns) and the potential distribution between the coil turns. A compensation structure scheme and a method for determining compensation parameters that can effectively improve the transmission capacity are adopted. This scheme significantly reduces the parasitic equivalent capacitance of the coil by changing the potential distribution between the coil turns, and improves the transmission performance and insulation performance. Moreover, an evaluation method using transfer admittance as a verification index is proposed. Experimental results show that compared with the traditional lumped compensation method, the output capacity of the system is increased by nearly ten times, which verifies the correctness and effectiveness of the method.**

***Index Terms*—Inter-turn structural capacitance, MHz-level MCR-WPT system, parasitic equivalent capacitance, transfer admittance.**

I. Introduction

MAGNETICALLY coupled resonant wireless power transfer (MCR-WPT) technology has garnered extensive research and applications in recent years [1]–[2]. Increasing the operating frequency of the system is an effective method to extend the transmission distance and reduce the volume of the WPT system [3]–[4].

However, when the operating frequency of the WPT system reaches the MHz range—for instance, 6.78 MHz (the wireless charging frequency specified by AirFuel)—capacitive parasitic parameters in the magnetically coupled coils will affect the transmission performance of the WPT system and thus cannot be ignored [5]–[6].

Clarifying the formation mechanism and mathematical model of parasitic capacitances in magnetically coupled coils is crucial for mitigating their impacts. Currently, the shortest path method, function method, and improved shortest path method are utilized in [7] to calculate the inter-turn structural capacitances of transformers under high-frequency (HF) conditions. [8] introduces a calculation method for the parasitic capacitance of HF solenoid inductors, which are formed by uniformly winding single-layer coils with a circular cross-section on a cylindrical non-conductive magnetic core. In [9], an analytical method based on conformal transformation is proposed to solve the inter-turn structural capacitances and turn-to-core capacitances of coils with different geometric structures. In [10], the total parasitic capacitance is calculated based on the approximate solution of inter-turn structural capacitances. Existing studies have analyzed the impacts and calculation methods of inter-turn structural capacitances between adjacent turns in transformers and inductors, but they have neglected the influence of inter-turn structural capacitances between non-adjacent turns on the equivalent parasitic capacitance.

To optimize the transmission performance of magnetically coupled coils, [11] utilizes the parasitic capacitance of the coils as part of the compensation capacitance. However, this method is only applicable to the parallel/parallel (P/P) compensation topology and not to other topologies such as series/series (S/S), series/parallel (S/P), and series/series-parallel (S/SP) [12]–[15]. [16]–[17] suggest paralleling multiple multi-layer PCB coils to generate large inter-turn structural capacitance for replacing compensation capacitors, thereby improving the reliability of magnetically coupled coil design. Nevertheless, the compensation method that leverages parallel resonance between inter-turn structural capacitance and the equivalent inductance of the coil is only suitable for current-source-driven P/P compensation topologies, not for voltage-source-driven compensation networks such as the S/S topology. Among these studies, [16] addresses this issue by adopting a traditional centralized series compensation capacitor on the transmitter side, but the equivalent parasitic capacitance of the transmitter side still impairs the transmission capability of the magnetically coupled

Manuscript received December 2, 2025; revised February 3, 2026; accepted March 3, 2026. Date of publication June 30, 2026; date of current version April 28, 2026. This work was supported in part by the China National Science Foundation under the grant 51407032 and Fujian Provincial Natural Science Foundation of China under the grant 2019J01251. (*Corresponding Author: Qingbin Chen.*)

All authors are with the College of electrical Engineering and Automation, Fuzhou University, Fuzhou 350108, China (e-mail: hq12138@126.com; chw@fzu.edu.cn; 240127095@fzu.edu.cn; 715749116@qq.com; cqb@fzu.edu.cn).

Digital Object Identifier 10.24295/CPSSTPEA.2026.000010

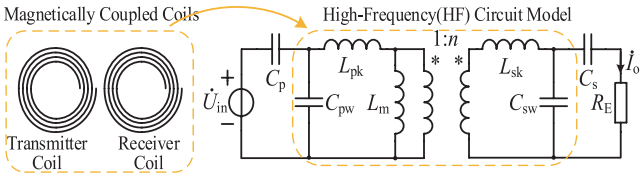

Fig. 1. S/S compensation tank with consideration for parasitic capacitance.

coils. [18] utilizes the inter-turn structural capacitance as the sectional compensation capacitance to achieve a compact coil structure; however, the adjustable range of the inter-turn capacitance is limited by the coil structure and insulating material, and the proximity effect loss will increase significantly under high-frequency conditions. The series sectional compensation method adopted in [19]–[20] employs compensation capacitors with the same capacitance value. Among them, the number of compensation capacitors in [19] is four times the number of coil turns, resulting in a complex compensation structure and insufficient compensation accuracy.

To address the aforementioned issues, this paper first analyzes the impact of parasitic capacitance on the transmission performance of magnetically coupled coils under S/S compensation. A mathematical model of the equivalent parasitic capacitance of magnetically coupled coils accounting for both adjacent and non-adjacent inter-turn structural capacitances is established, and the key factors affecting the equivalent parasitic capacitance are clarified. Subsequently, a compensation topology scheme capable of effectively enhancing the transmission capability of magnetically coupled coils is proposed. This scheme modifies the inter-turn potential distribution of the coils to reduce their equivalent parasitic capacitance, and a method for determining the compensation parameters is provided. By utilizing series resonance between the compensation capacitor and the decoupled equivalent inductance of each turn, the scheme can be applied to voltage-source-driven S/S compensation topologies, solving the problem that equivalent parasitic capacitance and inter-turn structural capacitance, when used as parallel compensation capacitors, cannot be employed in S/S compensation topologies.

In addition, at an operating frequency of 6.78 MHz, traditional evaluation methods judge the improvement in the transmission capability of magnetic coupling structures by measuring the overall efficiency of the WPT system. However, at HF, the parasitic parameters of other components in the circuit significantly affect the system's energy transfer characteristics, masking the performance of the magnetic coupling structure itself and making accurate evaluation difficult. This paper innovatively proposes an evaluation method for magnetically coupled coils using a network analyzer to measure transadmittance. This method directly and accurately characterizes the suppression effect of the equivalent parasitic capacitance of the magnetically coupled coils themselves and the degree of optimization of their transmission performance, providing a quantitative basis for the design and improvement of magnetic coupling structures in HF WPT systems.

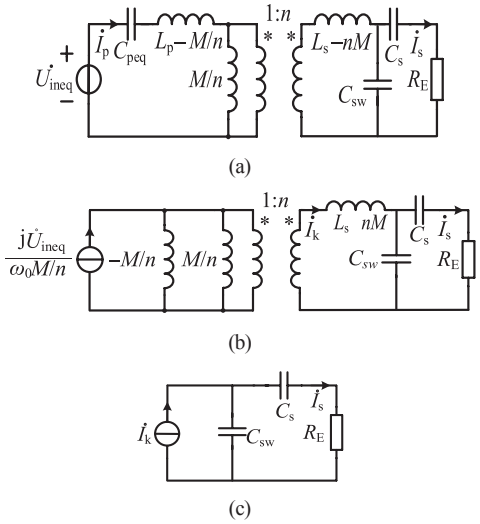

Fig. 2. Circuit equivalent transformation of S/S compensation with parasitic capacitance. (a) Thevenin equivalent transformation of the circuit in Fig. 1. (b) Equivalent transformation diagram of the power supply. (c) Equivalent transformation diagram of the receiving side.

II. Analysis of the Impact of Parasitic Capacitance in Magnetically Coupled Coils

A. Analysis of the Impact of Equivalent Parasitic Capacitance of Coils on Transmission Performance

In the series/series (S/S) capacitance compensation topology, the compensation capacitor at the transmitter side is only related to the parameters of the transmitting coil, independent of factors such as load magnitude and coil mutual inductance. However, this scenario changes in HF (6.78 MHz) circuits. This paper first analyzes the impact of parasitic capacitance on such compensation circuits through the HF model of magnetically coupled coils.

L_{pk} and L_{sk} are the leakage inductances of the transmitting coil and receiving coil, respectively; L_m is the magnetizing inductance; C_{pw} and C_{sw} are the equivalent parasitic capacitances of the transmitting-side and receiving-side coils; C_p and C_s are the series compensation capacitors at the transmitting side and receiving side; R_E is the equivalent load resistance; $\dot{U}_{in}$ is the input voltage source; n is the equivalent turns ratio.

Performing Thevenin equivalent transformation on Fig. 1, its model parameters are replaced by the self-inductances L_p, L_s and mutual inductance M shown in Fig. 2(a) [14]. Among them, the equivalent voltage source $\dot{U}_{ineq}$ and equivalent capacitance C_{peq} can be expressed as:

$$\begin{cases} \dot{U}_{ineq} = \dfrac{\dot{U}_{in} C_p}{C_p + C_{pw}} \\ C_{peq} = C_p + C_{pw} \end{cases} \tag{1}$$

The condition $1/\omega_0 C_{peq} = \omega_0 L_p$ defines the resonant angular frequency ω_0 of the equivalent capacitance C_{peq} and the transmitting coil inductance L_p. Under this condition, after performing Thevenin equivalent transformation on the inductor and voltage

source as shown in Fig. 2(b), the parallel combination of $-M/n$ and M/n results in infinite impedance. Through primary-secondary side conversion, the equivalent circuit in Fig. 2(c) is obtained.

The equivalent current source of the receiving-side coil $\dot{I}_k$:

$$\dot{I}_k = \frac{j\dot{U}_{ineq}}{\omega_0 M} \tag{2}$$

The output current of the magnetically coupled receiving-side coil $\dot{I}_s$:

$$\dot{I}_s = \dot{I}_k \frac{1/j\omega_0 C_{sw}}{1/j\omega_0 C_{sw} + 1/j\omega_0 C_s + R_E} \tag{3}$$

Combining (1), (2), and (3), the magnitude of the output current $|\dot{I}_s|$ of the magnetically coupled coil is obtained as:

$$\begin{cases} |\dot{I}_s| = \dfrac{|\dot{U}_{in}|}{\omega_0 M(1+\alpha)\sqrt{(1+\beta)^2 + (\omega_0 C_{sw} R_E)^2}} \\ \alpha = \dfrac{C_{pw}}{C_p},\ \beta = \dfrac{C_{sw}}{C_s} \end{cases} \tag{4}$$

(4) indicates that the magnitude of the output current of the magnetically coupled receiving-side coil is related to C_{pw} and C_{sw}. At this point, the output current no longer exhibits load independence but is instead related to the equivalent load resistance R_E.

In summary, the parasitic capacitance of the magnetically coupled coils is a key factor affecting their transmission performance. In the circuit, it is mainly reflected in their ability to convert the input excitation voltage $\dot{U}_{in}$ at the input side of the coils into the output current $\dot{I}_s$ at the output side. Excessively large equivalent parasitic capacitance will reduce the output current, thereby degrading the system's transmission performance. Therefore, the transmission performance of the magnetic coupling structure can be defined as the ratio between the output current and the input excitation voltage $\dot{U}_{in}$.

B. Evaluation Method for Magnetically Coupled Coils

As magnetically coupled coils serve as the key pathway for energy transfer in WPT systems, it is crucial to accurately evaluate their transmission capability. This paper proposes an evaluation method for magnetically coupled coils using a network analyzer to measure transadmittance.

In the two-port network of magnetically coupled coils, the transadmittance Y_T describes the relationship between the current response on the receiving side and the voltage excitation on the transmitting side. Its mathematical expression is:

$$Y_T = \frac{\dot{I}_s}{\dot{U}_{in}} \tag{5}$$

Combining (4) and (5), the magnitude of the transadmittance Y_T is:

$$\begin{cases} |Y_T| = \dfrac{1}{\omega_0 M(1+\alpha)\sqrt{(\omega_0 C_{sw} R_E)^2 + (1+\beta)^2}} \\ \alpha = \dfrac{C_{pw}}{C_p},\ \beta = \dfrac{C_{sw}}{C_s} \end{cases} \tag{6}$$

According to (5), when the input voltage $\dot{U}_{in}$ is constant, a higher transadmittance of the magnetically coupled coils corresponds to a larger output current $\dot{I}_s$. Under constant-current output characteristics, an increase in output current implies an improvement in the system's output power. Thus, transadmittance can be used to characterize the enhancement of the transmission capability of magnetically coupled coils. Further analysis of (6) shows that transadmittance also reflects the improvement of the coils' parasitic capacitance. When the structure of the magnetically coupled coils remains unchanged, the compensation capacitors C_p and C_s also remain unchanged. In this case, a smaller equivalent parasitic capacitance of the coils results in a larger transadmittance. Measuring the transadmittance can effectively reflect the improvement of the coils' equivalent parasitic capacitance, providing an important basis for evaluating the transmission performance and optimizing the design of magnetic coupling systems.

Since network analyzers measure the *S*-parameters of two-port networks, conversion to *Y*-parameters is required based on the definition of *S*-to-*Y* parameter transformation, as shown in (7):

$$\begin{cases} Y_T = \dfrac{\dot{I}_s}{\dot{U}_{in}} = \dfrac{-2S_{21}(R_{01}R_{02})^{1/2}}{ab+c} \\ a = (Z_{01}^* + S_{11}Z_{01}) \\ b = (R_E - R_E S_{22} + Z_{02}^* + S_{22}Z_{02}) \\ c = S_{12}S_{21}Z_{01}(R_E - Z_{02}) \end{cases} \tag{7}$$

where S_{12}, S_{21}, S_{11}, and S_{22} are the two-port parameters measured by the network analyzer; R_{01} and R_{02} are the real parts of the impedances at ports 1 and 2 of the network analyzer, respectively; Z_{01} and Z_{02} are the impedances at ports 1 and 2; Z_{01}^* and Z_{02}^* are the complex conjugates of Z_{01} and Z_{02}.

C. Evaluation Method for Magnetically Coupled Coils

Since non-adjacent turns are far apart and the middle-layer turns provide a certain shielding effect, existing studies have neglected the influence of capacitance between non-adjacent turns [8]. However, according to (8) for calculating the parasitic equivalent capacitance of the coil based on the energy method, the magnitude of the parasitic equivalent capacitance is also related to the voltage between turns. Given the large voltage difference between non-adjacent turns, the electric field energy stored by the structural capacitance between non-adjacent turns cannot be ignored.

$$W_t = \frac{1}{2} C_{pw} U_p^2 \tag{8}$$

where W_t denotes the total electric field energy stored in the

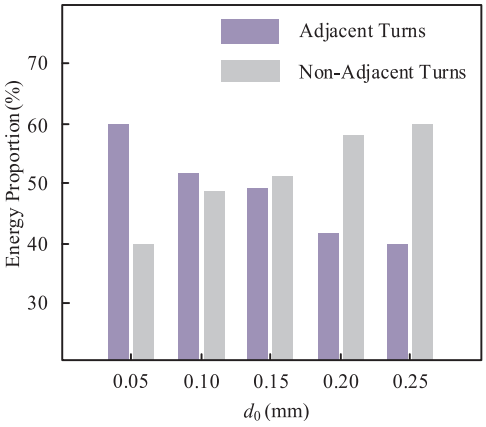

Fig. 3. Proportion of electric field energy distribution of the coil.

entire coil, C_{pw} represents the parasitic equivalent capacitance of the transmitting coil, and U_p is the voltage across the transmitting coil.

ANSYS 3D simulation software is employed to analyze the inter-turn energy distribution of the magnetically coupled coils illustrated in Fig. 3. The total electric field energy between adjacent turns (W_{at}) and the total electric field energy between non-adjacent turns (W_{nat}) are calculated using (9).

$$\begin{cases} W_{at} = \sum_{i=1}^{N-1} \frac{1}{2} C_{i(i+1)} U_{i(i+1)} \\ W_{nat} = \sum_{i=1}^{N-2} \frac{1}{2} C_{i(i+2)} U_{i(i+2)} + \cdots + \sum_{i=1}^{1} \frac{1}{2} C_{i(i+N-1)} U_{i(i+N-1)} \end{cases} \tag{9}$$

Fig. 3 shows the electric field energy distribution under different turn spacings d_0.

As can be seen from the figure above, with the increase of the coil turn spacing d_0, the proportion of electric field energy between non-adjacent turns in the total energy gradually increases, even exceeding that between adjacent turns. Therefore, establishing a calculation model that considers the structural capacitance between non-adjacent turns is of practical significance.

III. Analysis of Parasitic Capacitance Generation Mechanism in Magnetically Coupled Coils

Parasitic capacitances C_{pw} and C_{sw} are equivalent capacitances determined by the electric field energy stored in magnetically coupled coils, which are related to the inter-turn structural capacitance and potential distribution of the coils. This paper conducts analysis based on coreless planar spiral coils.

Due to the structure of spiral coils, their electric field distribution is nearly symmetric. The electric field energy dθ stored in the infinitesimal dW_1 of the 1st turn is:

$$\mathrm{d}W_1 = \sum_{j=2}^{N} dW_{1j} = \sum_{j=2}^{N} \frac{1}{2} \mathrm{d}q_{1j} \cdot U_1(\theta) \tag{10}$$

As shown in Fig. 4, where dq_{1j} denotes the charge induced

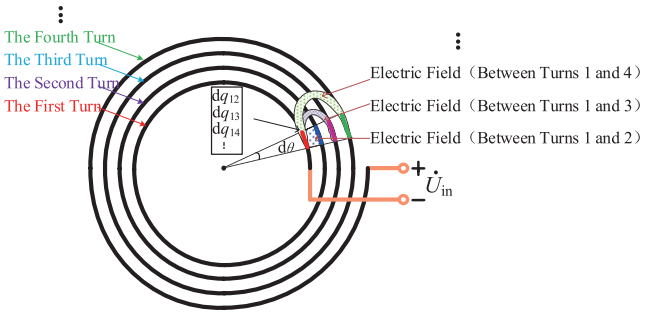

Fig. 4. The induced charge on the 1st turn in dθ.

on the 1st turn by the electric field between the 1st turn and the jth turn within the range of infinitesimal dθ, and $U_1(\theta)$ is the potential distribution along the θ direction on the 1st turn.

Therefore, the total electric field energy stored in the 1st turn is:

$$W_1 = \int_0^{2\pi} \sum_{j=2}^{N} \frac{1}{2} \mathrm{d}q_{1j} \cdot U_1(\theta) \tag{11}$$

The total electric field energy W_t stored in the entire coil is:

$$W_t = \sum_{i=1}^{N} W_i = \sum_{i=1}^{N} \int_0^{2\pi} \sum_{j=2}^{N} \frac{1}{2} \mathrm{d}q_{ij} \cdot U_i(\theta) \tag{12}$$

Owing to the symmetry of planar spiral coils, the distribution of induced charges is nearly uniform, so dq_{ij} can be calculated as follows:

$$\mathrm{d}q_{ij} = \frac{q_{ij}}{2\pi} \mathrm{d}\theta \tag{13}$$

Combining (12) and (13), W_t is:

$$W_t = \sum_{i=1}^{N} \int_0^{2\pi} \sum_{j=2}^{N} \frac{1}{2} U_i(\theta) \cdot \frac{q_{ij}}{2\pi} \mathrm{d}\theta \tag{14}$$

As can be seen from Fig. 1, the total electric field energy stored in the entire coil can also be calculated using (8). Thus, the parasitic capacitance C_{pw} can be derived:

$$C_{pw} = \frac{1}{U_p^2} \sum_{i=1}^{N} \int_0^{2\pi} \sum_{j=2}^{N} U_i(\theta) \frac{q_{ij}}{2\pi} \cdot \mathrm{d}\theta \tag{15}$$

According to (15), C_{pw} is related to the induced charge of each turn and the potential distributed along each turn. To calculate C_{pw}, it is necessary to analyze the induced charge of each turn and the potential distribution along each turn. The induced charge of the i-th turn can be calculated as follows:

$$\begin{aligned} q_i &= q_{i1} + q_{i2} + \cdots + q_{ii} + \cdots + q_{iN} \\ &= C_{i1}U_{i1} + C_{i2}U_{i2} + \cdots + C_{ii}U_{ii} \cdots + C_{iN}U_{iN} \end{aligned} \tag{16}$$

where C_{i1} and U_{i1} (i = 1, 2, 3…, N) represent the capacitance and voltage between the i-th turn and the 1st turn, respectively. C_{ii} and U_{ii} are the capacitance and voltage between the i-th turn and the ground. Since the magnetically coupled system is a charge-balanced system and grounding does not need to be

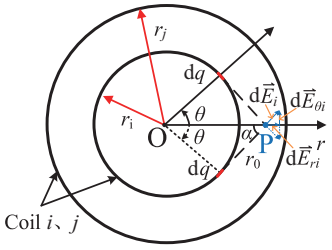

Fig. 5. Equivalent structure of two-turns planar spiral coil.

considered, C_{ii} and U_{ii} can be neglected.

A. Calculation Method for Structural Capacitance Between Adjacent and Non-Adjacent Turns

For planar spiral coils, they can be simplified to concentric circular coils when calculating the inter-turn structural capacitance. The simplified schematic diagram is shown in Fig. 5. Simulation analysis using ANSYS 3D shows that the error caused by this simplification is less than 2.55%.

Assume the charges in the i-th turn and j-th turn of the winding are Q and –Q, respectively. In polar coordinates, if the distance between two wires is much larger than the wire diameter, the influence of the wire diameter can be ignored, and the wires can be equivalent to electric axes. At this time, the electric field intensity generated by the charge infinitesimal dq in the i-th turn can be calculated using (17):

$$\begin{cases} \mathrm{d}\vec{E}_i = \dfrac{\mathrm{d}q}{4\pi\varepsilon_0 r_0^2}\vec{e} \\ \mathrm{d}q = Q\dfrac{\mathrm{d}\theta}{2\pi} \\ r_0 = \sqrt{r_i^2 + r^2 - 2r_i r\cos(\theta)} \end{cases} \tag{17}$$

Due to the symmetry of the coil, the θ-component of the electric field $\mathrm{d}\vec{E}_{\theta i}$ intensity cancels each other out, leaving only the r-component. The r-component of the electric field $\mathrm{d}\vec{E}_i$ intensity generated by the i-th turn is:

$$\begin{cases} \mathrm{d}\vec{E}_{ri} = \mathrm{d}E_i\cos(\alpha)\vec{e}_r \\ \cos(\alpha) = \dfrac{r_0^2 + r^2 - r_i^2}{2r_0 r} \\ \vec{E}_{ri} = \displaystyle\int_0^{2\pi}\mathrm{d}\vec{E}_{ri} \\ \vec{E}_r = \vec{E}_{ri} + \vec{E}_{rj} \\ \quad = \displaystyle\int_0^{2\pi}\frac{Q\left[r - r_i\cos(\theta)\right]}{8\pi^2\varepsilon_0[r_i^2 + r^2 - 2r_i r\cos(\theta)]^{1.5}}\mathrm{d}\theta + \\ \quad \displaystyle\int_0^{2\pi}\frac{-Q\left[r - r_j\cos(\theta)\right]}{8\pi^2\varepsilon_0[r_j^2 + r^2 - 2r_j r\cos(\theta)]^{1.5}}\mathrm{d}\theta \end{cases} \tag{18}$$

Using (19), the voltage difference between the i-th turn and j-th turn can be obtained, and then the structural capacitance C_{ij} between the i-th turn and j-th turn can be derived:

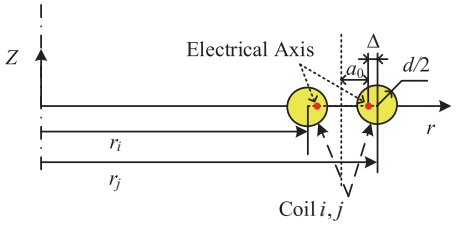

Fig. 6. Electric axis analysis considering coil conductor diameter.

$$\begin{cases} U_{ij} = \displaystyle\int_{r_i+d/2}^{r_j-d/2}\vec{E}_r\mathrm{d}r \\ C_{ij} = \dfrac{Q}{U_{ij}} \end{cases} \tag{19}$$

By combining (17), (18), and (19), C_{ij} can be simplified to:

$$C_{ij} = \{\int_{r_i+d/2}^{r_j-d/2}\int_0^{2\pi}\frac{\left[r - r_i\cos(\theta)\right]}{8\pi^2\varepsilon_0[r_i^2 + r^2 - 2r_i r\cos(\theta)]^{1.5}}\mathrm{d}\theta + \int_0^{2\pi}\frac{-\left[r - r_j\cos(\theta)\right]}{8\pi^2\varepsilon_0[r_j^2 + r^2 - 2r_j r\cos(\theta)]^{1.5}}\mathrm{d}\theta\mathrm{d}r\}^{-1} \tag{20}$$

However, in many applications, spiral coils are tightly wound with small inter-turn distances, so the wire diameter cannot be ignored, as shown in Fig. 6.

Based on the electric axis method, and replacing the charge effect of the circular conductor with two slender electric axes, the position of the electric axis of the winding turn can be calculated as follows:

$$\begin{cases} a_0 = \sqrt{(\dfrac{r_j - r_i}{2})^2 - (\dfrac{d}{2})^2} \\ \Delta = \dfrac{r_j - r_i}{2} - a_0 \end{cases} \tag{21}$$

where d is the diameter of the coil wire.

Therefore, considering the influence of the conductor diameter, the r-component of the electric field intensity between the i-th turn and j-th turn of the winding is:

$$\begin{aligned} \vec{E}_r &= \vec{E}_{ri} + \vec{E}_{rj} \\ &= \int_0^{2\pi}\frac{Q[r - (r_i + \Delta)\cos(\theta)]}{8\pi^2\varepsilon_0[(r_i + \Delta)^2 + r^2 - 2(r + \Delta)r\cos(\theta)]^{1.5}}\mathrm{d}\theta + \\ &\int_0^{2\pi}\frac{-Q[r - (r_j - \Delta)\cos(\theta)]}{8\pi^2\varepsilon_0[(r_j - \Delta)^2 + r^2 - 2(r_j - \Delta)r\cos(\theta)]^{1.5}}\mathrm{d}\theta \end{aligned} \tag{22}$$

In summary, the inter-turn structural capacitance C_{ij} is given by:

$$C_{ij} = \{\int_{r_i+d/2}^{r_j-d/2} (\int_0^{2\pi}\frac{[r - (r_i + \Delta)\cos(\theta)]}{8\pi^2\varepsilon_0[(r_i + \Delta)^2 + r^2 - 2(r_i + \Delta)r\cos(\theta)]^{1.5}}\mathrm{d}\theta +$$

$$\int_0^{2\pi} \frac{-[r-(r_j-\Delta)\cos(\theta)]}{8\pi^2\varepsilon_0[(r_j-\Delta)^2+r^2-2(r_j-\Delta)r\cos(\theta)]^{1.5}}\mathrm{d}\theta)\mathrm{d}r\}^{-1} \tag{23}$$

For actual magnetically coupled systems, the inter-turn structural capacitance between any two turns in a multi-turn coil is affected by other turns. Thus, in this paper, a new method is proposed to calculate the inter-turn structural capacitance of multi-turn concentric circular coils.

The charge matrix for the multi-turn concentric circular coil structure is shown in (24):

$$\begin{bmatrix} q_1 \\ q_2 \\ q_3 \\ \vdots \\ q_{N-1} \\ q_N \end{bmatrix} = \begin{bmatrix} 0 & C_{12} & C_{13} & \cdots & C_{1(N-1)} & C_{1N} \\ C_{21} & 0 & C_{23} & \cdots & C_{2(N-1)} & C_{2N} \\ C_{31} & C_{32} & 0 & \cdots & C_{3(N-1)} & C_{3N} \\ \vdots & \vdots & \vdots & \ddots & \vdots & \vdots \\ C_{(N-1)1} & C_{(N-1)2} & C_{(N-1)3} & \cdots & 0 & C_{(N-1)N} \\ C_{N1} & C_{N2} & C_{N3} & \cdots & C_{N(N-1)} & 0 \end{bmatrix} \cdot \begin{bmatrix} 0 & U_{21} & U_{31} & \cdots & U_{(N-1)1} & U_{N1} \\ U_{12} & 0 & U_{32} & \cdots & U_{(N-1)2} & U_{N2} \\ U_{13} & U_{23} & 0 & \cdots & U_{(N-1)3} & U_{N3} \\ \vdots & \vdots & \vdots & \ddots & \vdots & \vdots \\ U_{1(N-1)} & U_{2(N-1)} & U_{3(N-1)} & \cdots & 0 & U_{N(N-1)} \\ U_{1N} & U_{2N} & U_{3N} & \cdots & U_{(N-1)N} & 0 \end{bmatrix} \tag{24}$$

If the charge of each turn is known, the electric field intensity distribution and the voltage between any two turns can be calculated. Therefore, N equations can be derived from $N(N-1)$ capacitance variables to solve all capacitance variables. In addition, it is necessary to assume $N-1$ groups of different turn charge distributions, which are shown in (25):

$$[q]_{\langle k\rangle} = \begin{bmatrix} 0 & \cdots & 0 & q_k = Q & q_{k+1} = -Q & 0 & \cdots & 0 \end{bmatrix}^{\mathrm{T}} \quad \{k \mid k < N \quad and \quad k \in N_+\} \tag{25}$$

where $[q]_{\langle k\rangle}$ is the k-th case of the charge distribution on the coil. Furthermore, the voltage between adjacent turns under any charge distribution can be calculated as follows:

$$\begin{cases} U_{k(k+1)} = \int_{r_k+d/2}^{r_{k+1}-d/2} \{\int_0^{2\pi} \frac{Q[r-(r_k+\Delta)\cos(\theta)]}{8\pi^2\varepsilon_0[(r_k+\Delta)^2+r^2-2(r_k+\Delta)r\cos(\theta)]^{1.5}}\mathrm{d}\theta + \int_0^{2\pi} \frac{-Q[r-(r_{k+1}-\Delta)\cos(\theta)]}{8\pi^2\varepsilon_0[(r_{k+1}-\Delta)^2+r^2-2(r_{k+1}-\Delta)r\cos(\theta)]^{1.5}}\mathrm{d}\theta\}\mathrm{d}r \\ U_{\mathrm{m(m+1)}\ 1\le m<\mathrm{N},\mathrm{m}\ne k} = \int_{r_m+d/2}^{r_{m+1}-d/2} \{\int_0^{2\pi} \frac{Q[r-r_k\cos(\theta)]}{8\pi^2\varepsilon_0[r_k^2+r^2-2r_k r\cos(\theta)]^{1.5}}\mathrm{d}\theta + \int_0^{2\pi} \frac{-Q[r-r_{k+1}\cos(\theta)]}{8\pi^2\varepsilon_0[r_{k+1}^2+r^2-2r_{k+1}r\cos(\theta)]^{1.5}}\mathrm{d}\theta\}\mathrm{d}r \end{cases} \tag{26}$$

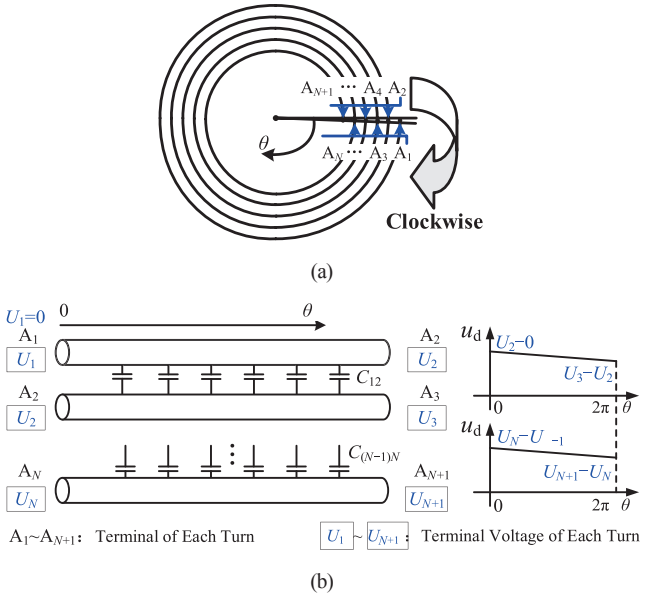

Fig. 7. Voltage potential distribution of the spiral coil without cores. (a) Schematic diagram of the unfolded magnetic-core-free planar spiral coil. (b) Analysis the inter-turn voltage between two adjacent turns.

According to Kirchhoff's voltage law, the voltage between non-adjacent turns can be calculated using the voltage between adjacent turns. By combining (24), (25), and (26), the inter-turn structural capacitance C_{ij} can be obtained. For example, the capacitance parameters corresponding to q_1 can be expressed as follows:

$$\begin{bmatrix} C_{12} \\ C_{13} \\ \vdots \\ C_{1(N-1)} \\ C_{1N} \end{bmatrix} = \begin{bmatrix} U_{12_{\langle 1\rangle}} & U_{13_{\langle 1\rangle}} & \cdots & U_{1(N-1)_{\langle 1\rangle}} & U_{1N_{\langle 1\rangle}} \\ U_{12_{\langle 2\rangle}} & U_{13_{\langle 2\rangle}} & \cdots & U_{1(N-1)_{\langle 2\rangle}} & U_{1N_{\langle 2\rangle}} \\ \vdots & \vdots & \vdots & \vdots & \vdots \\ U_{12_{\langle N-2\rangle}} & U_{13_{\langle N-2\rangle}} & \cdots & U_{1(N-1)_{\langle N-2\rangle}} & U_{1N_{\langle N-2\rangle}} \\ U_{12_{\langle N-1\rangle}} & U_{13_{\langle N-1\rangle}} & \cdots & U_{1(N-1)_{\langle N-1\rangle}} & U_{1N_{\langle N-1\rangle}} \end{bmatrix}^{-1} \begin{bmatrix} q_{1_{\langle 1\rangle}} \\ q_{1_{\langle 2\rangle}} \\ \vdots \\ q_{1_{\langle N-2\rangle}} \\ q_{1_{\langle N-1\rangle}} \end{bmatrix} \tag{27}$$

where $q_{1\langle k\rangle}$ is the charge amount of q_1 in the k-th case of the charge distribution on the coil; $U_{12\langle k\rangle}\ldots U_{1N\langle k\rangle}$ are the inter-turn voltages under the k-th charge case.

B. Calculation Method for Parasitic Equivalent Capacitance of Magnetically Coupled Coils

For coreless planar spiral coils as shown in Fig. 7. Fig. 7(b) shows the clockwise unwrapping of Fig. 7(a), illustrating the inter-turn potential difference distribution. Here, U_1, U_2, U_3 ... U_{N+1} represent the potentials at both ends of each turn, and the potential difference between adjacent turns can be approximated as the voltage difference at the left end of each turn.

$$U_{ij}(\theta) \approx U_j - U_i \tag{28}$$

Therefore, the induced charge q_{ij} in the i-th turn is:

$$q_{ij} \approx C_{ij}(U_j - U_i) \tag{29}$$

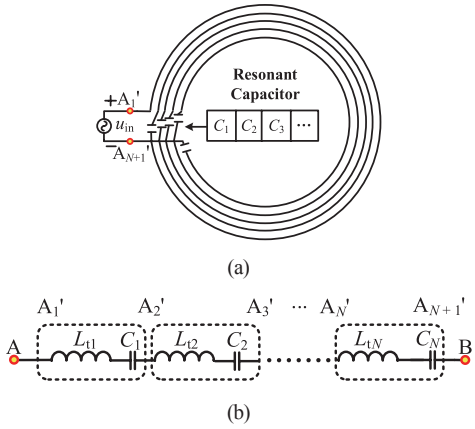

Fig. 8. Capacitance compensation structure. (a) Distributed capacitor compensation structure. (b) Unfolded equivalent circuit diagram.

Combining (14) and (29), the total electric field energy W_t stored in the coil is:

$$W_t = \frac{1}{2}C_{pw}U_{N+1}^2 \approx \sum_{j=1}^{N}[\sum_{\substack{i=1,\\ i\neq j}}^{N}\frac{1}{2}\frac{C_{ij}(U_j-U_i)}{2\pi}\int_0^{2\pi}U_j(\theta)\mathrm{d}\theta] \quad (30)$$

Since the potential of each turn is linearly distributed, it can be known that:

$$\int_0^{2\pi}U_j(\theta)\mathrm{d}\theta = \frac{U_j+U_{j+1}}{2}\cdot 2\pi \quad (31)$$

By simplifying (30), the parasitic equivalent capacitance C_{pw} of the coil can be derived:

$$C_{pw} \approx \frac{1}{2U_{N+1}^2}\sum_{j=1}^{N}\sum_{i=1,i\neq j}^{N}[C_{ij}(U_j-U_i)\cdot(U_j+U_{j+1})] \quad (32)$$

The above indicates that the magnitude of the parasitic equivalent capacitance is related to the inter-turn potential difference.

IV. Optimization Method for Parasitic Equivalent Capacitance of Magnetically Coupled Coils

From the above analysis, when the structure of the magnetically coupled coil cannot be changed (i.e., the inter-turn structural capacitance remains constant), reducing the potential difference between each turn of the coil to decrease the parasitic equivalent capacitance is an effective method to improve the transmission performance of the multi-turn coil structure.

A. Compensation Structure for Enhancing Transmission Capability of Magnetically Coupled Coils

This paper proposes a capacitance compensation structure as shown in Fig. 8(a) and presents a method for determining the compensation capacitance parameters. By using this method, the voltage difference between different turns can be reduced.

Therefore, this paper proposes to resonate the compensation capacitor of each turn with the decoupling equivalent inductance L_{ttxi} of the same turn, thereby reducing the voltage difference between A_1' and A_2', A_2' and A_3', …, A_N' and A_{N+1}'.

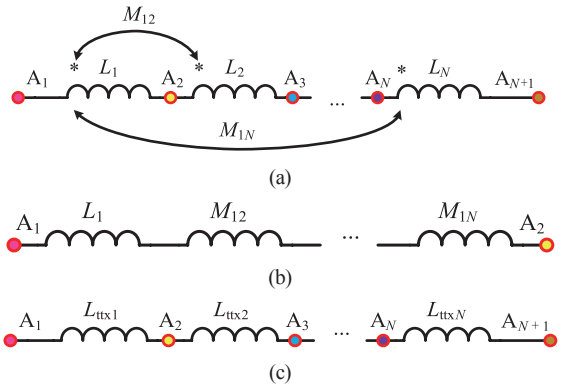

Fig. 9. Decoupling equivalent circuit analysis of the coil. (a) Schematic diagram of the *N*-turn coupled coil. (b) Equivalent circuit diagram of the 1st decoupled coil. (c) Equivalent circuit diagram of the *N*-turn decoupled coil.

TABLE I
Basic Parameters of the Magnetically Coupled Coil

Physical Parameters of the Coil			
D_i	inner diameter of coil	38 cm	
D_o	outer diameter of coil	40 cm	
N_{tx}	number of turns of transmitting coil	5 turns	
N_{rx}	number of turns of receiving coil	5 turns	
	wire diameter	1 mm	
	transmission distance	13 cm	
Electrical Structure of Coil			
		lumped compensation	distributed compensation
L_p	self-inductance of transmitting coil	26.796 μH	27.314 μH
L_s	self-inductance of receiving coil	26.655 μH	26.860 μH
M	mutual inductance	3.708 μH	3.946 μH
k	coupling coefficient	0.138	0.146

When the two resonate, the voltage difference between adjacent turns is:

$$\dot{U}_{A_i\_A(i+1)'} = \dot{U}_{L_{ttxi}} + \dot{U}_{C_i} = 0 \quad (33)$$

(33) shows that this method can significantly reduce the voltage difference between adjacent turns of the coil. Additionally, the parasitic equivalent capacitance of the magnetically coupled coil will be reduced to 0.

B. Method for Determining Compensation Parameters

As described in the previous section, this paper reduces the parasitic equivalent capacitance of the magnetically coupled coil by resonating the compensation capacitance of each turn with the decoupled equivalent inductance L_{ttxi} of each turn.

$$L_{ttxi} = L_i + \sum_{\substack{j\neq i,\\ j=1}}^{N-1} M_{ij} \quad (34)$$

TABLE II
COMPARISON OF THE INTER-TURN STRUCTURAL CAPACITANCE RESULTS OF THE MAGNETICALLY COUPLED COIL

Capacitance value	Simulation	Theoreticcal	Capacitance value	Simulation	Theoreticcal
C_{12}/pF	19.021	18.776	C_{23}/pF	16.898	16.054
C_{34}/pF	17.263	16.232	C_{45}/pF	19.604	19.465
C_{13}/pF	3.844	4.823	C_{24}/pF	2.8658	3.6856
C_{35}/pF	3.932	4.9765	C_{14}/pF	2.3163	2.5097
C_{25}/pF	2.4461	2.5627	C_{15}/pF	3.4819	2.6632

TABLE III
COMPARISON OF THE EQUIVALENT PARASITIC CAPACITANCE RESULTS OF THE MAGNETICALLY COUPLED COIL

Equivalent parasitic capacitance	Theoretical calculation	FEA simulation	Measurement
C_{pw}	8.721 pF	8.765 pF	9.257 pF
C_{pw}	8.721 pF	8.765 pF	9.101 pF

where L_i is the self-inductance of each turn, and M_{ij} is the mutual inductance between the i-th turn and j-th turn in the coil. Its equivalent circuit is shown in Fig. 9(a), and the decoupled equivalent circuit of the first turn is shown in Fig. 9(b). The same method can be used for decoupling other turns. The decoupled equivalent circuit of the entire coil is shown in Fig. 9(c). The decoupled equivalent inductance of each turn of the coil is shown in Fig. 9:

The self-inductance and mutual inductance of the coil can be obtained.

The mutual inductance M_{ij} can be expressed by (36):

$$M_{ij}=\frac{\psi_{ij}}{I_j}=\frac{\mu_0}{4\pi}\oint_{l_2}\oint_{l_1}\frac{\mathrm{d}\vec{l}_1\cdot\mathrm{d}\vec{l}_2}{R} \tag{35}$$

where $\mathrm{d}\vec{l}_1$ and $\mathrm{d}\vec{l}_2$ are the length infinitesimals element of coil i and j, respectively; R is the distance of $\mathrm{d}\vec{l}_1$ and $\mathrm{d}\vec{l}_2$:

$$\begin{cases}\mathrm{d}\vec{l}_1=(-r_i\sin\varphi\vec{e}_{\mathrm{x}}+r_i\cos\varphi\vec{e}_{\mathrm{y}})\mathrm{d}\varphi\\ \mathrm{d}\vec{l}_2=(-r_j\sin\theta\vec{e}_{\mathrm{x}}+r_j\cos\theta\vec{e}_{\mathrm{y}})\mathrm{d}\theta\\ R=\sqrt{\left(r_i\cos\varphi-r_j\cos\theta\right)^2+(r_j\sin\theta+t-r_i\sin\varphi)^2+h^2}\end{cases} \tag{36}$$

Combining (36) and (37), the mutual inductance M_{ij} is:

$$M(r_i,r_j,t,h)=\frac{\mu_0}{4\pi}\int_0^{2\pi}\int_0^{2\pi}\frac{r_ir_j\cos(\theta-\varphi)}{R} \tag{37}$$

In summary, the decoupled equivalent inductance L_{ttxi} can be expressed as:

$$\begin{cases}L_{\mathrm{ttxi}}=\sum_{j=1,i\neq j}^{N}M(r_i,r_j,0,0)+L_i(r_i)\\ L_i(r_i)\approx(\mu_0/8\pi)\cdot 2\pi r_i\end{cases} \tag{38}$$

TABLE IV
DISTRIBUTED CAPACITANCE COMPENSATION PARAMETERS

Transmitting coil		Receiving coil	
L_{ttxi}	C_i	L_{ttxi}	C_i
5.280 μH	104.280 pF	5.204 μH	105.881 pF
5.670 μH	97.190 pF	5.518 μH	99.860 pF
5.722 μH	96.308 pF	5.580 μH	98.757 pF
5.632 μH	97.840 pF	5.486 μH	100.442 pF
5.225 μH	105.458 pF	5.087 μH	108.33 pF

where L_i is the internal self-inductance of the coil.

In conclusion, when the equivalent decoupled inductance L_{ttxi} of each turn of the coil is known, the compensation capacitance parameter value for each turn in the optimization scheme of the magnetically coupled coil can be determined.

V. EXPERIMENTAL VERIFICATION

To verify the correctness of the theoretical analysis and optimization scheme, this paper conducts experiments on the magnetically coupled coils shown in Fig. 4 using a vector network analyzer (KEYSIGHT E5072A, bandwidth: 30 kHz~4.5 GHz), a signal generator (Agilent 33522A), an impedance analyzer (WK65120B, bandwidth: 20 Hz~120 MHz), and a power amplifier (AR 600A225A, bandwidth: 10 kHz~225 MHz).

The electrical parameters in Table I are measured using an impedance analyzer. At 6.78 MHz, the compensation capacitance values are measured by the impedance analyzer, with a compensation error ranging from 1% to 4%.

Based on the coil self-inductance, mutual inductance, and operating frequency, the compensation capacitances C_{p} = 10.779 pF and C_{s} = 11.164 pF for the lumped compensation scheme are calculated.

This paper verifies the calculation accuracy of the inter-turn capacitance using ANSYS, as presented in Table II. On the other hand, the correctness of the total equivalent parasitic capacitance C_{w} of the coil is validated through experimental measurements, as shown in Table III.

Using the inter-turn structural capacitance values in the above table and the electric field energy calculation in (8), the calculated value of the coil electric field energy W_{t} is 438.26 pJ, and the theoretical value is 436.04 pJ. Thus, the theoretical

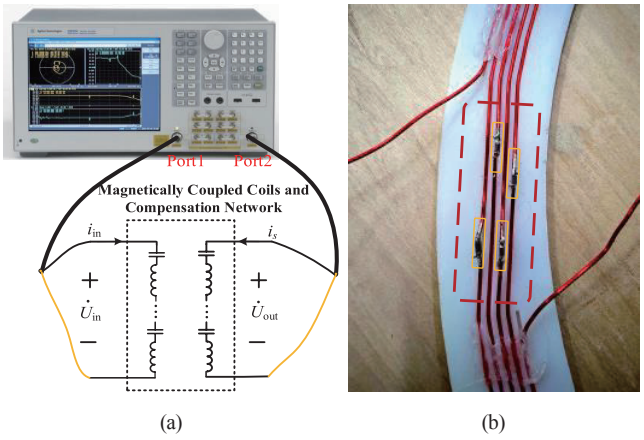

Fig. 10. Network analyzer measurement diagram. (a) Test schematic diagram. (b) Physical diagram of distributed capacitance compensation.

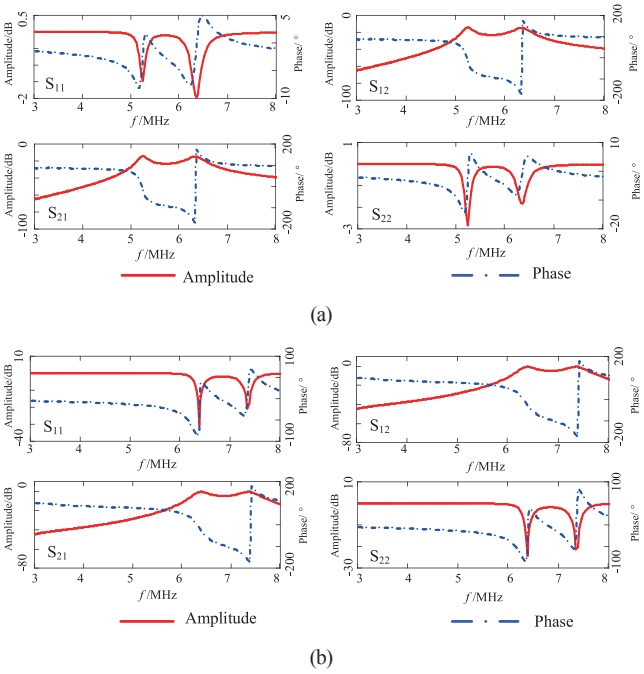

Fig. 11. *S*-parameter under different compensation. (a) Traditional lumped compensation scheme. (b) Distributed compensation scheme.

calculation value of the parasitic equivalent capacitance is obtained. The comparison results of the coil parasitic equivalent capacitance obtained by three methods are shown in Table III.

A. Vector Network Analyzer Measurement and Analysis

The two-port *S*-parameters of the magnetically coupled coil are measured using a vector network analyzer (the test setup is illustrated in Fig. 13), and the transadmittance Y_T of the magnetically coupled coil is obtained.

The S-parameter test results in Fig. 11 indicate that the resonance point of the improved magnetically coupled coil shifts from 5.1 MHz to 6.4 MHz, which means the parasitic equivalent capacitance is significantly reduced.

Fig. 12 shows the transfer admittance of magnetically coupled coils with different compensation structures calculated using (7) at 6.78 MHz. The results indicate that after distributed capacitance compensation, the transfer admittance is increased by nearly ten times, meaning the ability to convert input voltage into output current is greatly improved.

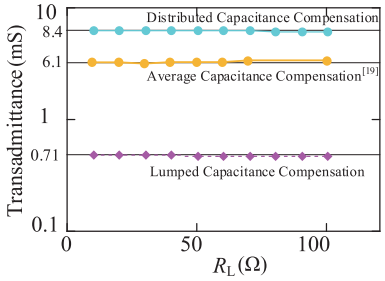

Fig. 12. Transfer admittance of the system under different compensation methods.

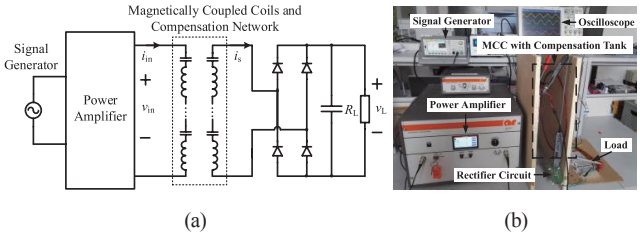

Fig. 13. Circuit connection diagram of the power amplifier. (a) Test circuit diagram. (b) Test experiment.

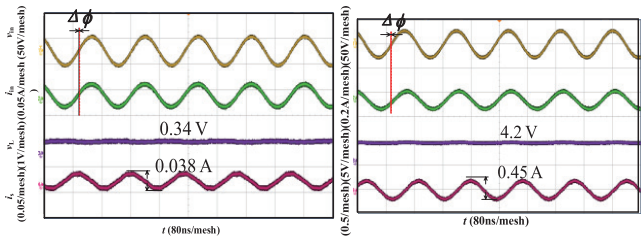

Fig. 14. Waveforms under different compensation. (a) Lumped compensation. (b) Distributed compensation.

B. Power Stage Voltage-Current Conversion Test

To verify the consistency between the transfer admittance measured by the vector network analyzer and that under actual operating conditions. A power voltage excitation of V_{in} = 20 V(f = 6.78 MHz) is applied to the transmitter side of the magnetically coupled coils to test the output characteristics of the traditional lumped and distributed compensation methods. The power stage experimental circuit connection and the experimental site are illustrated in Fig. 13, respectively.

The power amplifier experiment is used to test the output current i_s of the compensated magnetically coupled receiving coil and the input voltage v_{in} of the transmitting coil. The measured waveforms when the load resistance R_L = 30 Ω are shown in Fig. 14.

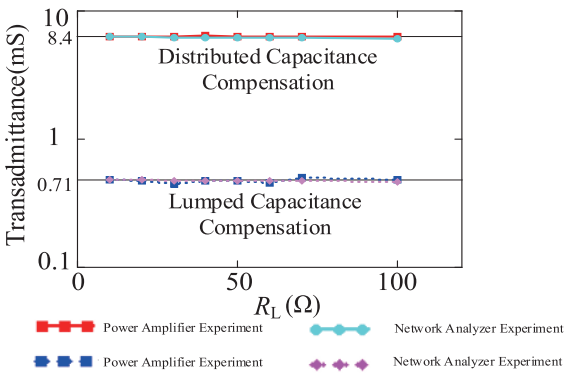

Fig. 15. Comparison diagram of the transfer admittance under two testing methods.

From the power amplifier experiment results in Fig. 14, under the same excitation voltage source, the input voltage and input current of the two compensation schemes are in the same phase, achieving zero-phase compensation. The energy transmitted by the magnetically coupled coil is mainly reflected in the active component on the load.

In the lumped compensation scheme, the peak-to-peak value of the output current i_s of the receiving coil is only 0.038 A, and the load voltage $v_L = 0.34$ V. In the distributed compensation scheme, the i_s of the receiving coil is increased to 0.45 A, and the load voltage $v_L = 4.2$ V. In addition, with the improved magnetically coupled coil, the transmission efficiency of the system is increased from 1.29% to 52.5%. The experiment shows that the voltage-current conversion capability of the optimized magnetically coupled coil is improved by nearly ten times, which is consistent with the evaluation method of measuring transfer admittance based on the vector network analyzer. This verifies the reliability of the method for evaluating the transfer admittance of the magnetically coupled structure using the vector network analyzer and the improvement effect of transmission performance.

It is worth noting that when calculating the voltage on the load using the average value of the i_s of the magnetically coupled receiving coil, the result is larger than the actually measured load voltage v_L. The reason is the introduction of a rectifier bridge and other components, and the HF parasitic parameters of these circuits also affect the output performance to a certain extent. Therefore, the traditional method of evaluating the transmission performance of the WPT system by the ratio of output power to input power cannot accurately reflect the improvement of the transmission performance of the magnetically coupled coil, while the evaluation index adopted in this paper does not introduce these errors.

In addition, the transfer admittances Y_T ($f = 6.78$ MHz) under the two test conditions are compared, and the results are shown in Fig. 15.

As can be seen from Fig. 15, the results measured by the vector network analyzer are in good consistency with those of the power amplifier experiment. This verifies that the method of measuring transfer admittance using the vector network analyzer can be effectively used to evaluate the transmission performance of magnetically coupled coils.

VI. Conclusions

For the S/S-type compensation circuit structure, this paper clarifies that in the MHz-level MCR-WPT system, the large parasitic equivalent capacitance is a key factor affecting the transmission performance of the magnetically coupled structure. It also points out that the electric field energy between non-adjacent turns is non-negligible compared with that between adjacent turns of the magnetically coupled coil. An accurate mathematical model of the equivalent parasitic capacitance of the magnetically coupled coil is established by considering the inter-turn structural capacitance and non-inter-turn structural capacitance. It is further pointed out that when the coil structure remains unchanged, the potential distribution of the winding is a key factor affecting the parasitic equivalent capacitance of the winding. Therefore, this paper adopts a compensation structure scheme and its parameter determination method that can effectively improve the transmission capability of the magnetically coupled coil to replace the traditional lumped compensation structure. The principle of this scheme is to minimize the electric field energy between coil turns by designing the inter-turn potential distribution, thereby reducing the parasitic equivalent capacitance and improving the transmission performance of the magnetically coupled coil under HF conditions. Finally, an evaluation method for measuring the transfer admittance of the magnetically coupled coil using a vector network analyzer is proposed. This method can effectively characterize the improvement of the parasitic equivalent capacitance and transmission performance of the coil, and significantly improve the simplicity and efficiency of the evaluation process of the magnetically coupled coil.

References

[1] A. Sun, C. Xia, Z. Yang, Q. Wang, Y. Chen, Z. Yang, and C. Wang, "Parameter identification technology of multi-frequency and multi-load MCR-WPT system based on HM-PWM control," in *Proceedings of the CSEE*, vol. 45, no. 20, pp. 8189–8202, Aug. 2025.

[2] G. Wei, L. Hao, Y. Zhang, and T. Zhang, "Completely analytical calculation of inductance for circular coils with bilateral finite magnetic cores at arbitrary position in WPT systems," in *IEEE Transactions on Power Electronics*, vol. 39, no. 6, pp. 6597–6602, Jun. 2024.

[3] W. Xie, W. Chen, Q. Chen, and Y. Jiang, "Compact anti-offset WPT system with dual-coupled SP-S compensation," in *Proceedings of the CSEE*, vol. 44, no. 2, pp. 714–725, Jan. 2024.

[4] Q. Chen, F. Fan, J. Wang, X. Zhang, W. Chen, and X. Dhen, "Accurate calculation method of rectifier load equivalent impedance based on S/SP compensation and inverter switching loss optimization," in *Proceedings of the CSEE*, vol. 42, no. 11, pp. 4138–4151, Jun. 2022.

[5] H. Zhao, Z. Tian, X. Zhang, Y. Qiu, L. Li, P. Chen, F. Yang, X. Wu, and G. Xu, "Nonresonant compensation optimization for efficiency improvement of wireless power transfer system with relay coil," in *IEEE Transactions on Power Electronics*, vol. 39, no. 2, pp. 2835–2845, Feb. 2024.

[6] A. Kurs, A. Karalis, R. Moffatt, J. D. Joannopoulos, P. Fisher, and M. Soljačić, "Wireless power transfer via strongly coupled magnetic resonances," in *Science*, vol. 317, no. 5834, pp. 83–86, Jul. 2007.

[7] Y. H. Sohn, B. H. Choi, E. S. Lee, G. C. Lim, G. -H. Cho, and C. T. Rim, "General unified analyses of two-capacitor inductive power transfer systems: equivalence of current-source SS and SP compensations," in *IEEE Transactions on Power Electronics*, vol. 30, no. 11, pp. 6030–6045, Nov. 2015.

[8] W. Xu, Z. Zhao, and Q. Jiang, "Calculation method for parasitic capacitance of high-frequency transformers," in *Journal of Tsinghua University (Science and Technology)*, vol. 61, no. 10, pp. 1088–1096, Feb. 2021.

[9] A. Ayachit and M. K. Kazimierczuk, "Self-capacitance of single-layer inductors with separation between conductor turns," in *IEEE Transactions on Electromagnetic Compatibility*, vol. 59, no. 5, pp. 1642–1645, Oct. 2017.

[10] J. Huang, Y. Dou, P. Wang, Z. Ouyang, and M. A. E. Andersen, "Inductance and parasitic capacitance modeling of spiral air-core inductor in MHz inductive power transfer system," in *2023 IEEE Applied Power Electronics Conference and Exposition (APEC)*, Orlando, FL, USA, 2023, pp. 75–81.

[11] L. Deng, Q. Sun, F. Jiang, S. Wang, S. Jiang, H. Xiao, and T. Peng, "Modeling and analysis of parasitic capacitance of secondary winding in high-frequency high-voltage transformer using finite-element method," in *IEEE Transactions on Applied Superconductivity*, vol. 28, no. 3, pp. 1–5, Apr. 2018.

[12] L. Gu, G. Zulauf, A. Stein, P. A. Kyaw, T. Chen, and J. M. R. Davila, "6.78-MHz wireless power transfer with self-resonant coils at 95% DC-DC efficiency," in *IEEE Transactions on Power Electronics*, vol. 36, no. 3, pp. 2456–2460, Mar. 2021.

[13] Z. Li, C. Zhang, J. Wang, Z. Wang, and S. Huang, "Research on constant current and constant voltage of WPT system based on variable frequency reconfiguration S/SP topology," in *Transactions of China Electrotechnical Society*, vol. 39, no. 15, pp. 4718–4732, Aug. 2024.

[14] M. Lu and K. D. T. Ngo, "Systematic design of coils in series–series inductive power transfer for power transferability and efficiency," in *IEEE Transactions on Power Electronics*, vol. 33, no. 4, pp. 3333–3345, Apr. 2018.

[15] X. Liu, R. Chen, F. Li, D. Zhou, and J. Zou, "A WPT system with DC-link series/parallel AC-link parallel rectifiers for AUVs with multiple charging voltages and currents," in *IEEE Transactions on Power Electronics*, vol. 39, no. 8, pp. 10605–10617, Aug. 2024.

[16] Q. Wang, M. A. Saket, A. Troy, and M. Ordonez, "A self-compensated planar coil for resonant wireless power transfer systems," in *IEEE Transactions on Power Electronics*, vol. 36, no. 1, pp. 674–682, Jan. 2021.

[17] Y. -D. Lee, K. -W. Kim, and G. -W. Moon, "A self-compensated planar coil with integrated single-switch regulator for wireless power transfer (WPT) systems," in *IEEE Transactions on Power Electronics*, vol. 36, no. 10, pp. 10954–10958, Oct. 2021.

[18] D. Kong, J. Zhao, L. Mao, Y. Yin, and J. Zhang, "Design and analysis of segmental compensation coils utilizing inter-turn capacitance in wireless power transfer systems" in *Transactions of China Electrotechnical Society*, vol. 40, no. 12, pp. 3803–3814, Jun. 2025.

[19] Y. Zeng, D. Qiu, X. Meng, B. Zhang, and S. C. Tang, "Optimized design of coils for wireless power transfer in implanted medical devices," in *IEEE Journal of Electromagnetics*, RF and Microwaves in Medicine and Biology, vol. 2, no. 4, pp. 277–285, Dec. 2018.

[20] J. H. Kim, B. -S. Lee, J. -H. Lee, S. -H. Lee, C. -B. Park, S. -M. Jung, S. -G. Lee, K. -P. Yi, and J. Baek, "Development of 1-MW inductive power transfer system for a high-speed train," in *IEEE Transactions on Industrial Electronics*, vol. 62, no. 10, pp. 6242–6250, Oct. 2015.

Qing He was born in Jiangxi, China, in 1999. He received the B.S. degree in Electrical Engineering and Automation from the Tiangong University, Tianjin, China, in 2022. Currently, he is pursuing a doctoral degree at Fuzhou University. His research interests include the suppression and diagnosis of electromagnetic compatibility and wireless power transfer technology.

Wei Chen received the M.S. and Ph.D. degrees in Electrical Engineering from Fuzhou University, Fuzhou, China, in 1987 and 1990, respectively. He was a Senior Visiting Professor with the Center for Power Electronics Systems (CPES), Virginia Tech, Blacksburg, VA, USA, from 1996 to 1998. He was a Research and Development Manager with Delta Electronics Company Ltd., and the Delta Power Electronics Center, Shanghai, China, from 1999 to 2008. He has authored or coauthored more than 80 technical articles, including IEEE Transactions and Proceedings. He held more than 40 approved patents from China and USA. His research interests include power conversion, high-frequency magnetic technology, EMI debug and solution, wireless power transfer, electromagnetic field analysis, and applications. Prof. Chen is an Executive Member of the Council of China Power Supply Society (CPSS).

Chezu Wang was born in Anhui, China, in 2001. He received the B.S. degree in Electrical Engineering and Automation from Xiamen University of Technology, Xiamen, China, in 2023. Currently, he is pursuing a master's degree at Fuzhou University.

Wei Qiu was born in Jiangxi, China, in 2000. He received the B.S. degree in Electrical Engineering and Automation from Xiamen University of Technology, Xiamen, China, in 2023. Currently, he is pursuing a master's degree at Fuzhou University.

Qingbin Chen received the B.E. and Ph.D. degrees in Electrical Engineering from Fuzhou University, Fuzhou, China, in 2007 and 2012, respectively. He was a visiting scholar with the University of Florida, Florida, USA, from 2017 to 2018. His research interests include high frequency magnetic technology, EMC diagnosis and suppression technology, and wireless power transfer. Dr. Chen is the member of Magnetic Components and Ferrite Materials (Magnetic Standards Committee of China) and served as the Vice chairperson and Deputy Secretary General of Magnetic Component Specialty Committee of CPSS.